

Fluorine Abundances of Galactic Low-Metallicity Giants

H. N. Li

Key Lab of Optical Astronomy, National Astronomical Observatories, Chinese Academy of
Sciences, A20 Datun Road, Chaoyang, Beijing 100012, China

lhn@nao.cas.cn

H.-G. Ludwig

Zentrum für Astronomie der Universität Heidelberg, Landessternwarte, Königstuhl 12, D-69117
Heidelberg, Germany

hludwig@lsw.uni-heidelberg.de

E. Caffau

Zentrum für Astronomie der Universität Heidelberg, Landessternwarte, Königstuhl 12, D-69117
Heidelberg, Germany

ecaffau@lsw.uni-heidelberg.de

N. Christlieb

Zentrum für Astronomie der Universität Heidelberg, Landessternwarte, Königstuhl 12, D-69117
Heidelberg, Germany

N.Christlieb@lsw.uni-heidelberg.de

and

G. Zhao

Key Lab of Optical Astronomy, National Astronomical Observatories, Chinese Academy of
Sciences, A20 Datun Road, Chaoyang, Beijing 100012, China

gzhao@nao.cas.cn

– 2 –

Received 2012 October 4; accepted 2013 January 15

Fluorine Abundances of Galactic Low-Metallicity Giants

ABSTRACT

With abundances and $2\text{-}\sigma$ upper limits of fluorine (F) in seven metal-poor field giants, nucleosynthesis of stellar F at low metallicity is discussed. The measurements are derived from the HF(1-0) R9 line at 23358 \AA using near-infrared K -band high-resolution spectra obtained with CRIRES at the Very Large Telescope. The sample reaches lower metallicities than previous studies on F of field giants, ranging from $[\text{Fe}/\text{H}] = -1.56$ down to -2.13 . Effects of three-dimensional model atmospheres on the derived F and O abundances are quantitatively estimated and shown to be insignificant for the program stars. The observed F yield in the form of $[\text{F}/\text{O}]$ is compared with two sets of Galactic chemical evolution models, which quantitatively demonstrate the contribution of Type II supernova (SN II) ν -process and asymptotic giant branch/Wolf-Rayet stars. It is found that at this low-metallicity region, models cannot well predict the observed distribution of $[\text{F}/\text{O}]$, while the observations are better fit by models considering an SN II ν -process with a neutrino energy of $E_\nu = 3 \times 10^{53}$ erg. Our sample contains HD 110281, a retrograde orbiting low- α halo star, showing a similar F evolution as globular clusters. This supports the theory that such halo stars are possibly accreted from dwarf galaxy progenitors of globular clusters in the halo.

Subject headings: Galaxy: halo — stars: abundances — stars: Population II

1. Introduction

Although fluorine is a very interesting element, its chemical evolution is not yet well understood. F has only one stable, yet fragile isotope, ^{19}F , which is easily destroyed in the stellar interiors by the most abundant elements, H and He, by means of the reactions $^{19}\text{F}(\text{p},\alpha)^{16}\text{O}$ and $^{19}\text{F}(\alpha,\text{p})^{22}\text{Ne}$. Theoretically, in order to explain the production of F, three sites have been proposed to explain the mechanism that enables it to escape from the hot stellar interior after it has been created, including Type II supernovae (SN II), asymptotic giant branch (AGB) stars, and Wolf-Rayet (WR) stars. It is predicted that SN II produce ^{19}F primarily as a result of neutrino spallation (Woosley & Haxton 1988; Woosley & Weaver 1995; Heger et al. 2005; Kobayashi et al. 2011a). For AGB stars, Forestini et al. (1992) proposed that ^{19}F is synthesized and then dredged up to the surface during the He-burning thermal pulses. In WR stars, ^{19}F is probably produced during the He-burning phase and then ejected into space by strong stellar winds before it is destroyed (Meynet & Arnould 2000).

There are very few atomic or molecular lines of F that are suitable for stellar abundance analysis. Current studies on F have focused on the measurement of the single HF molecular line at 23358 Å in cool stars. Jorissen et al. (1992) put up a pioneering work in the field by measuring the first F abundance of a number of giants with near-solar metallicities. Through the past decade, more studies on F nucleosynthesis have been carried out, aiming at various types of objects, including solar- and moderate-metallicity global cluster giants (Cunha et al. 2003; Werner et al. 2005; Smith et al. 2005), giants in the Galactic bulge (Cunha et al. 2008; Uttenthaler et al. 2008), AGB stars (Abia et al. 2009, 2010), and main-sequence dwarfs in the solar neighborhood (Recio-Blanco et al. 2012). Besides, detailed exploration of the chemical evolution of F has been carried out targeting chemically peculiar objects, such as cool extreme He stars (Pandey 2006), C-enhanced stars (Schuler et al. 2007; Lucatello et al. 2011), Ba stars (Alves-Brito et al. 2011), and even an extragalactic C-star (Abia et al. 2011).

With new nucleosynthesis yields and updated observations, chemical evolution models can now predict more details of the nucleosynthesis of F, but only the contribution of AGB stars to the F production has been observationally confirmed (Werner et al. 2005; Abia et al. 2010, 2011). The chemical evolution model for MilkyWay-like disk galaxies of Renda et al. (2004) suggests a scenario where AGB stars only began to contribute to the production of F after ~ 1 Gyr. This model states that AGB stars are at present the major contributors for the production of F; while in the early Galaxy, only SN II contribute to the F abundance, and provide a solution to the discrepancy between models and observed F abundance in Galactic giant in the intermediate-metallicity range. A more recent chemical evolution model targeting fluorine by Kobayashi et al. (2011a) adopts the ν -process yields and yields of AGB stars with $1 - 7 M_{\odot}$, based on the infall and star formation history in Kobayashi et al. (2011b). The model predicts a [F/O] plateau at low metallicity depending on the neutrino luminosity. The included ν -process enhances the predicted F abundances at higher metallicities, and helps to fit the high F abundances observed in field and bulge giants. Both models are in good agreement with observations in regions with solar or moderately low metallicities, indicating the importance for constraining the theoretical yields at low metallicity for further scrutiny and future observations. Alves-Brito et al. (2012) filled the gap at the low-metallicity area with M22 data, but the complex chemical enrichment history of this globular cluster leads to a large dispersion (0.6 dex) of the F abundances, thus does not follow the trend of other globular clusters or being explained by a general model. Hence, the metal-poor field giants in our observed sample, which have metallicities of $[\text{Fe}/\text{H}] < -1.5$, become very interesting in allowing us to map the pristine F abundance in earlier phases of the Galactic halo evolution.

Observations and data reduction, including the determination of stellar parameters and abundance analysis, are addressed in Sections 2 through 4. The three-dimensional (3D) effects on the abundances are described in Section 5. In Section 6, our results are discussed and interpreted, and a brief summary is given in Section 7.

2. CRIRES Observations

Seven metal-poor field giants were observed with CRIRES¹ (Cryogenic high-resolution Infrared Echelle Spectrograph; Kaeufl et al. 2004) at Very Large Telescope UT1 in a number of service runs from 2008 May through 2009 March. The slit width was set to 0".2, yielding the maximum resolution of 100,000 ($\sim 3 \text{ km s}^{-1}$). The four CCD chips cover the wavelength ranges from 22993 to 23118 Å, 23152 to 23273 Å, 23304 to 23420 Å, and 23450 to 23560 Å. Chip 3 includes the HF(1-0) R9 line which, in cool stars, has been verified to be most reliable for F abundance determination. The integration time was 30 s or 45 s for each nodding position per setting, and for two of the program stars, two exposures were obtained. A hot standard star with similar air mass was observed immediately either beforehand or afterward. The raw frames of science and standard objects were reduced with the CRIRES pipeline (v2.0.0), and after that, the science spectra were divided by corresponding standard star spectra to correct for the telluric lines and the illumination pattern, using the IRAF task Telluric. The typical signal-to-noise (S/N) ratio of the sample spectra around 23358 Å is higher than 200. Spectra of the HF line area for all exposures of our program stars are shown in Figure 1.

3. Atmospheric Parameters

The effective temperature T_{eff} and the surface gravity $\log g$ can be determined either spectroscopically or photometrically. The microturbulent velocity ξ is normally derived by removing any trend of abundances with equivalent widths of Fe lines. However, the fact that there is no Fe feature in the sample spectra within the coverage of CRIRES observation makes it difficult to independently determine the atmospheric parameters with the IR spectra alone. Thus, the stellar parameters for the sample stars were adopted from previously published data. Out of

¹<http://www.eso.org/instruments/crires>

a number of measurements, we relied on the work of Shetrone (1996), which includes all seven objects in our sample and thus provides a uniform set of atmospheric parameters. Moreover, it contains measurements of equivalent widths.

The model atmospheres adopted by Shetrone (1996) are taken from the grid of Bell et al. (1976), which is now outdated. Therefore, we have adopted the atmospheric parameters of Shetrone (1996) as the initial values, and further adjusted them with local thermal equilibrium (LTE) one-dimensional (1D) models computed with ATLAS9 (Kurucz 1994). The adjustment followed the traditional spectroscopic method. T_{eff} was adjusted to make Fe I lines with low excitation potential yield the same abundances as those with high excitation potential; the microturbulent velocity was adjusted until strong Fe I lines yield same abundances as weak Fe I lines; and $\log g$ was adjusted so that abundances from Fe I and Fe II lines were forced to agree with each other. The equivalent width (EW) of the Fe lines were directly adopted from the measurements of Shetrone (1996). The adjusted parameters do not differ much from Shetrone (1996)'s values, with a difference being 10 ± 45 K for T_{eff} , -0.03 ± 0.08 for $\log g$ and -0.02 ± 0.03 for [Fe/H].

Similarly, with the EW measurement and the linelist of Shetrone (1996), abundances of O, Mg, Al, and Eu (which cannot be determined from CRIRES spectra since no corresponding line features are present in the *K*-band spectra) were also re-calculated, using the ATLAS9 atmospheric models. The re-derived abundances show overall agreement with Shetrone's values, e.g., with a difference of 0.10 ± 0.08 for O, 0.10 ± 0.06 for Mg, -0.09 ± 0.07 for Al, and 0.06 ± 0.06 for Eu, respectively. The adopted atmospheric parameters and abundances, based on the optical data, are listed in Table 1.

4. Abundance Analysis

Using the spectrum synthesis code MOOG (Snedden 1973) and model atmospheres calculated with ATLAS9 (Kurucz 1994), LTE Na, C, and F abundances (and upper limits) were obtained by comparison with CRIRES spectra. The mixing-length parameter was set to $\alpha_{\text{MLT}} = 1.25$, and no convective overshooting was adopted. The wavelength range of the CRIRES spectra covers a few Phillips system C₂ lines; however, since our sample stars are of rather low-metallicities and without carbon enhancement (except for HD 135148), no C₂ line was detected. Therefore, we relied on the O abundances obtained as previously described, and derived the C abundances by fitting several ¹²C¹⁶O first overtone vibrational-rotational lines (2–0 and 3–1 vibration series). Although Shetrone (1996) also provides measurements of Na abundances, which was determined as an average of the abundances derived from EWs for the 6154 Å and 6160 Å NaI lines and from synthetic spectrum fits to the 5682 Å and 5688 Å NaI lines. there are two objects without Na EW measurements in the literature. However, there are two Na lines located at 23379 Å, which are strong and clean enough to measure the Na abundance with the IR spectra. The left plot of Figure 2 compares Na abundances determined from CRIRES spectra and re-derived from the EWs measured by Shetrone (1996) for the five stars with EW measurements, and the right plot compares the CRIRES Na abundances with the average Na abundances given by Shetrone (1996). The measurements agree within their uncertainties, and the CRIRES values are adopted for the following discussion.

The F abundances of our sample stars were determined by fitting the unblended HF (1–0) R9 line at 23358 Å. Out of the seven sample objects, clear HF R9 features were detected in two of them, HD 110281 and HD 135148, as shown in Figure 3. Note that HD 135148 is a spectroscopic binary with a companion star with the approximate mass of a white dwarf (e.g., Carney et al. 2003), it is thus not likely that the detected HF feature is reflecting the closeby CO lines from the companion stellar spectra. To confirm this, we have also checked the auto-correlation of the

spectra, and found no significant second peak associated with a companion star. For the remaining five spectra, $1\text{-}\sigma$ upper limits of F abundances were obtained, adopting the statistical error of EW based on the classical formula of Cayrel (1988):

$$\langle \Delta W^2 \rangle^{1/2} \simeq 1.6(w\Delta x)^{1/2}\epsilon \quad (1)$$

where w is the FWHM of the line; Δx refers to the sampling step of the spectra, and ϵ to the reciprocal spectral S/N in the case of normalized spectra. Considering the fact that the HF line is weak in the CRIRES spectra, we can estimate their expected FWHM from weak CO lines close to the HF line. The S/N of the spectra were calculated from several continuum regions on the same CCD as the HF feature. Note that except for the spectroscopic binary HD 135148, two other objects, HD 003008 and HD 110281 clearly show broader lines than other program stars. Spectroscopic and photometric observations by Carney et al. (2003) have concluded that the line-broadening of these two stars is caused by fast rotation rather than stellar companions, and also proposed the idea that these two rapid rotators show enhanced mass loss which is aided by the rotation, or by the addition of both orbital energy and angular momentum from an accreted planet to the stellar envelope. We have also investigated the detectability of HF lines with various EWs/upper limits, e.g., the difference in $A(F)$ between the two exposures of HD 110281 corresponds to a 1-2 mÅ difference in EW, which is on the same level as the $1\text{-}\sigma$ upper limit. We have adopted $2\text{-}\sigma$ upper limits of $A(F)$ in the following discussion, to ensure the possible detection considering the typical S/N and line widths of our program stars.

For the only C-enhanced star HD 135148, the ratio of $^{16}\text{O}/^{17}\text{O}$ was derived based on three $^{12}\text{C}^{17}\text{O}$ lines in our spectra, at 23347 Å, 23357 Å, and 23379 Å. A $^{16}\text{O}/^{17}\text{O}$ ratio of 140 ± 50 was derived. This oxygen isotope ratio is higher than normal at such a metallicity, if one only considers the nucleosynthesis of massive stars. However, since ^{17}O can be overproduced by AGB stars, and AGB stars can be the typical companion star that transfers nucleosynthesis products to the C-enhanced star, the high ratio of $^{16}\text{O}/^{17}\text{O}$ can be explained by this scenario. Note that the $^{12}\text{C}^{17}\text{O}$

line at 23357 Å is located right to the blue wing of the HF R9 line, but is not at all affecting the derived F abundance, as testified in early work like Abia et al. (2009). The fitted $^{12}\text{C}^{17}\text{O}$ line is also shown in Figure 3. For the synthetic fitting, we have adopted the Na linelist from Kurucz (1994), the CO linelist from Goorvitch (1994), and the HF linelist from Cunha et al. (2003). Validity of the linelist has been checked by fitting the *K*-band spectra of α Boo from the atlas of Hinkle et al. (1995).

The uncertainties of the abundance of F and other elements mainly comes from two aspects: the statistical error in the line equivalent widths, and the uncertainties of the atmospheric parameters. To estimate the former, statistical errors of the EW measurements were calculated adopting Equation 1, and the latter were determined by individually varying stellar parameters to measure their separate effects on the derived abundances. Typically, e.g., for HD 110281, the 1- σ EW error leads to an uncertainty of 0.02 dex of the F abundance, $\Delta T_{\text{eff}} = +100$ K leads to an increase of +0.25 of the F abundance, $\Delta \log g = +0.5$ produces $\Delta A(F) = -0.02$, and $\Delta \xi = +0.5$ km s $^{-1}$ gives a negligible $\delta A(F) < 0.001$. As for the Na abundance, the typical sensitivities to EW errors and atmospheric parameters are $\Delta A(\text{Na}) = +0.06, +0.07, -0.03$, and -0.01 respectively. The resulting uncertainties are then summed in quadrature to obtain the total statistical errors. For stars with more than one exposure, i.e., HD 110281 and [S84] 2643, abundances for the exposure with higher S/N was adopted, and the differences between the derived element abundances from different exposures turned out to be negligible. The derived abundances of C, O, F, Na, Mg, Al, and Eu are listed in Table 1.

5. 3D effects

5.1. Abundance Corrections for the HF R9 and Forbidden O Lines

It is well-known that atmospheres of metal-depleted, late-type stars are prone to exhibit significant deviations from radiative equilibrium (Asplund et al. 1999). In particular, abundances derived from molecular species can experience large corrections (e.g., González Hernández et al. 2008). From this perspective it is desirable to quantify the 3D effects – at least for fluorine and oxygen. Unfortunately, we have no 3D models available at the rather low gravities of our program stars. To nevertheless derive an estimate of the abundance corrections, we took four 3D models from the CIFIST atmosphere grid (Ludwig et al. 2009) at higher gravity and inspected the trend of the abundance corrections with changing T_{eff} and $\log g$. When calculating the abundance corrections, we followed the methodology described in Caffau et al. (2011). In the 3D models we assumed a solar chemical composition scaled to a metallicity of $[M/H] = -2.0$, with an enhancement of the α -elements by +0.4 dex.

Table 2 summarizes the results for the HF R9 line, and the two forbidden oxygen lines at 6300 Å and 6363 Å. The listed 3D abundance corrections are evaluated for weak lines (negligible saturation) – a good approximation considering the typical line strength. When running the 3D models, sufficient statistics were gathered so that residual statistical uncertainties on the abundance corrections are smaller than the accuracy to which they are given in the table. For completeness, we mention that in the 1D hydrostatic comparison models we assumed a mixing-length parameter of $\alpha_{\text{MLT}} = 1.0$ (close to what was adopted in the ATLAS9 models), and in the related 1D spectral synthesis calculations a microturbulence of $\xi = 2.0 \text{ km s}^{-1}$. However, both aspects have hardly any impact on the result. The corrections in Tab. 2 suggest that for the low-gravity giants of our sample, minor 3D effects are to be expected. Only at gravities $\log g > 2$ we expect substantial corrections (> 0.1 dex) on the F abundance at $[M/H] = -2$. For the HF line, mainly horizontal inhomogeneities (as opposed to differences in the vertical stratification) are the cause of the

changes of its strength in 3D compared to 1D models.

Digressing for the moment, we note that the abundance corrections obtained for the forbidden oxygen lines are not fully compatible with the corrections obtained by Collet et al. (2007). These authors obtained ≈ -0.1 dex at $T_{\text{eff}} = 5050$ K, $\log g = 2.2$, $[M/H] = -2.0$, and $[O/Fe] = +0.5$. Even considering that the atmospheric parameters are not exactly the same in their and our models, the corrections of Collet and collaborators appear noticeably larger. This is also the case for other species (see Ivanauskas et al. 2010; Dobrovolskas et al. 2010) and the reason is not yet understood.

Nevertheless, we proceed under the assumption that 3D corrections are insignificant for the F and O abundances we derived for our program stars.

5.2. Convective Line Shifts of HF and CO Lines

We used the cores of strong CO lines as synthesized by a 1D spectral synthesis code to correct for the imperfections of the wavelength calibration provided by the CRIRES reduction pipeline. One might ask whether convective line shifts alter the wavelength position of the cores significantly with respect to their laboratory wavelength. Again, we do not have fully adequate 3D models available for our target stars. We nevertheless used the 3D model from the CIFIST grid which gets closest ($T_{\text{eff}} = 3886$ K, $\log g = 1.0$, $[M/H] = -2.0$) to calculate line bisectors of the HF R9 line and a prototypical CO line in the HF region. We varied the strength of the lines by (artificially) varying the oscillator strength; in the case of the CO line this means that the variation was done at fixed C/O ratio. Figures 4 and 5 illustrate the outcome. The perhaps surprising result is that the magnitude of the convective shifts is very modest, not exceeding 250 m s^{-1} . The cores of strong CO lines in our target stars have typically a residual flux around 0.7, i.e., the HF line is weak. Differential shifts between their cores are even significantly less, unlikely to exceed

100 m s^{-1} corresponding to $\approx 8 \text{ m\AA}$ at the wavelength of the CRIRES spectra – much smaller than the line width. We conclude that our wavelength correction procedure should produce reliable line positions for the HF and CO lines, as can be seen in Figure 1.

6. Discussion

With the measurements of F abundances and upper limits of the program stars, it is now possible to probe the behavior of F evolution of field giants with low metallicities. Figure 6 displays the kinematic properties of our program stars. Please note that the radial velocity and proper motion data are directly obtained from previous literatures as listed in the database of SIMBAD². As can be seen, one of the stars with clear HF detections, HD 110281, is identified as a halo star with retrograde rotation, and another program star, BD +01 2916, is classified as a thick disk star. The sensitivities of the F abundances are checked along temperatures, and abundances of C, O, and Fe, as shown in Figure 7. Relevant correlations or dependencies have been addressed in a number of articles, including observations (Jorissen et al. 1992; Cunha et al. 2003; Abia et al. 2009), as well as theoretical predictions from Galactic chemical evolution models such as Renda et al. (2004) and Kobayashi et al. (2011a). We would expect for giant stars to find a correlation between the abundance of F and the abundances of O and Fe, and that the F abundances could be enhanced by stars exhibiting C-enhancement. It is quite likely that potential trends as expected are present in the comparisons, but we cannot draw firm conclusions on this since our sample size is small and we have obtained mostly upper limits only. Nevertheless, it is clear that HD 110281, the object with the highest F abundance, is the star with the lowest T_{eff} in our sample, and showing the highest metallicity (Fe and O). The HF molecule formation is very sensitive to temperature, hence T_{eff} is expected to set the level of upper limits on the F abundance.

²<http://simbad.u-strasbg.fr/simbad/>

The other star with a HF-detection, HD 135148, is showing notably higher C abundances compared to other program stars, since it is a CH-star as shown by Carney et al. (2003) and Shetrone et al. (1999). The observed trend of the F abundances with metallicity tracers suggest that O and Fe may be used as a reference on the detection limit of F; however, it is not clear to us whether there is a lower limit of F detection determined by the stellar metallicity, because Alves-Brito et al. (2012) has studied several M22 giants with metallicities (and stellar parameters) that are comparable to our sample but most of their giants’ spectra show measurable HF features. Note that these spectra based on which the Alves-Brito et al. (2012) derive the F abundances do not present higher resolution or S/N than our sample spectra; therefore, it is suspected that the different detection fraction of HF features between the two samples are possibly due to the fact that one is in clusters while the other is in the field.

In Figure 8, [F/O] abundance ratios treated as the indicator of the F yield of the sample, are plotted against [O/H] and [O/Fe] and compared with model predictions and previous observations. Two sets of models are selected, including Renda et al. (2004, R04 hereafter) which for the first time quantitatively demonstrated the contribution of AGB and WR stars to the F production, and the latest model by Kobayashi et al. (2011a, hereafter K11), who calculate the contribution of the ν -process of SN II and hypernovae (HN) to the nucleosynthesis of fluorine. Three model variants are constructed in R04: MWa (thick solid line) with SN II as the only source of ^{19}F , MWb (thick dotted line) including yields from both SN II and WR stars, and MWc (thick dashed line) including all three sources of SN II, WR, and AGB stars. For all three cases, R04 have considered that neutrino spallation is largely dominant in fluorine production, and they adopted the SN II yields of Woosley & Weaver (1995), which assumes a total energy in neutrinos of $E_\nu = 3 \times 10^{53}$ erg. As for K11, five cases are included: evolution with neither AGBs nor ν -process (SN II/Ia + HN, triple-dot-dashed line), chemical evolution with AGB contributions (SN II/Ia + HN + AGB, dashed line), the model for globular clusters with ν -process (dash-dotted line), ν -process of SN II and HN (dash-dotted and solid lines) with neutrino luminosity of $E_\nu = 3 \times 10^{53}$ erg and

$E_\nu = 9 \times 10^{53}$ erg respectively. Note, that K11 models do not include yields of WR stars, because the contribution by WR to F may be reduced by including rotation in the stellar models. For more details of the models, we refer the interested readers to R04 and K11.

As can be seen in Figure 8, for all cases taking ν -process into account, all models predict a plateau of [F/O] at low metallicity with $[O/H] \leq -1.2$, as proposed by K11. The ν -process remarkably enhances the level of F production compared to models without ν -process and indicates the dominant contribution from neutrino spallation to producing F in the early stage of Galactic evolution. For all four model variants with the same neutrino energies of $E_\nu = 3 \times 10^{53}$ erg, the predictions of the F production at the plateau of the models of R04 and K11 agree well with each other. For a better judgment of the significance of the differences between our observations and the model predictions, $1-\sigma$ error bars are also included to the upper limits of [F/O] of the sample. As C-enhanced stars are believed to be s-process enhanced and producers of F, the CH-star HD 135148 shows the highest F abundances as shown in Table 1, thus is not included in Figure 8 which intends to compare with the general trend. Also noted, due to its different kinematical properties from the rest of the sample, HD 110281 (shown in filled circle) may not follow the Galactic halo evolution, hence should be separately considered when compared with models. Except for these two objects, all upper limits of the other five objects in our sample (as shown with lower triangular) are located around the predicted plateau of R04 and the SN II ν -process model of K11, while well below the HN model of K11 with $E_\nu = 9 \times 10^{53}$ erg. The general trend of the observed [F/O] with increasing metallicity, and the apparent discrepancy between the observed [F/O] and predictions by models without neutrino spallation, suggest that a contribution of the ν -process is needed to explain the early production of F in the Galactic halo. The program stars with intermediate F content in the sample tend to follow the evolution model for SN II ν -process of K11 and the early phase of R04 models, which predict a similar "plateau", but program stars with low F upper limits are distributed at relatively lower level of [F/O], and cannot be explained by these models.

Our observed F abundances are also compared with previous observations, including giants of globular clusters (Cunha et al. 2003; Smith et al. 2005; Yong et al. 2008; Alves-Brito et al. 2012), the Milky Way bulge (Cunha et al. 2008), as well as K and M field giants (Cunha et al. 2003; Cunha & Smith 2005). As shown in the left panel of Figure 8, for globular cluster giants with comparable metallicity, e.g., M22 (Alves-Brito et al. 2012), the detected F level shows clear difference from our program stars, which could be explained by the different chemical enrichment history of field and cluster stars, and/or the wide range of chemical abundance variations of M22 due to its complex formation history. Previously available data of field giants covered only metallicities close to solar, thus they show a notably higher F abundances than our metal-deficient field giants. Apart from the field and globular cluster halo giants, Milky Way bulge giants (Cunha et al. 2008) are also compared. They are showing remarkably higher F abundances with a large scatter, which is difficult to explain by yields of current models. This also implies a different evolution of this central component of the Milky Way. However, it is interestingly noticed that HD 110281 follows very similar trend of [F/O] as giants in globular clusters such as M4, NGC6712, and ω Cen. Note in Table 1 that this object also shows rather low Na and Mg abundances, as well as being on a retrograde orbit in Figure 6, thus it is very likely a "low- α " halo star as defined by Nissen & Schuster (2010, 2011). As they have found based on the abundance and kinematic analysis, the less-bound low- α stars are probably accreted from dwarf galaxies with relatively slow star-formation, and some of them may be associated with the progenitor galaxy of globular clusters, including ω Cen, which could refer to a similar or relevant chemical evolution, hence explain the similarity in F evolution of HD 110281 and the compared globular cluster giants. Future observations of abundances of F and other elements of similar objects would be very interesting and important to obtain a deeper understanding of the origin of the dual halo of the Galaxy.

The timescale of SN II is much shorter than that of AGB or WR stars, which naturally explains that SN II dominate the area with lower [F/O] and higher [O/Fe], whereas AGB stars

start to notably contribute after $[O/H] > -1.5$ and become more important at higher metallicity and higher $[F/O]$. Therefore, the F abundance is a good clock to distinguish the contribution from low-mass AGB stars and SN II. It is true that based on our comparisons, none of the included models could well fit or predict the observations at lower metallicities, neither for field giants nor globular clusters. But it is also true that both the R04 and K11 models are originally aimed at better fitting the observational data of globular clusters at intermediate metallicities and giants toward solar metallicity due to the availability of observational data. This is also the reason why the observed F production from AGB stars is better explained, while there is still little known about the early evolution of F dominated by massive stars or the different F evolution of halo field giants and globular clusters stars. Future observations of field stars at low metallicities are crucial for further constraining models for such early stages of the Galactic chemical evolution, e.g., the neutrino luminosity released from SN II, and the initial conditions of the chemical evolution models for the older halo.

7. Summary and conclusion

With CRIRES observations of seven halo field giants at $[Fe/H] < -1.5$ and $[O/H] < -1.1$, and abundances of O, Mg, Al, and Eu determined in optical spectra from the literature, we have investigated the nucleosynthesis of their F content, and for the first time, explored the evolution of F in field giants in the low-metallicity regime. Among the program stars, the HF R9 feature is detected in two cases, HD 110281 and HD 135148, and $2\text{-}\sigma$ upper limits are estimated for the F abundance of the other stars. Using CIFIST model atmospheres, the 3D effect on the F and O abundance with comparable stellar parameters to the program stars are estimated, showing that for our sample, the corrections are negligible. The sensitivity of the F abundance/upper limits are also checked against T_{eff} , metallicities, O, and C. A correlation can be found between the upper limits of F and T_{eff} , which confirms the expectation that more stringent limits can be obtained

for cooler stars, and C-enhancement or higher metallicity are also enhancing the F abundance or upper limits. Galactic chemical evolution models by Renda et al. (2004) and Kobayashi et al. (2011a) predict a similar F production at low metallicity, and are compared with observations. It is suggested that the ν -process is necessary to explain the F production at the early stages of Galactic evolution, but the predicted [F/O] ratios do not fit well the observed distribution, whereas the observed trend is closest to the SN II model of Kobayashi et al. (2011a) and early phases of Renda et al. (2004) models with a low total energy in neutrinos, $E_\nu = 3 \times 10^{53}$ erg. Combined with kinematics, HD 110281 is identified as a low- α star (Nissen & Schuster 2010) with retrograde rotation. The consistent F nucleosynthesis of this star with the globular cluster halo stars support the scenario that this kind of objects may be accreted from nearby dwarf galaxies and enriched by early metal-deficient SN II. Future observations and modifications on models on relevant elements of the Galactic halo are important to achieve a better understanding of the above-mentioned results and remaining puzzles.

This work was supported by NSFC grant Nos. 11233004, 11103030, and 10903012, the Global Networks program of Universität Heidelberg, and grant CH 214/5-1 of Deutsche Forschungsgemeinschaft (DFG). We further acknowledge support by Sonderforschungsbereich SFB 881 "The Milky Way System" (subprojects A4 and A5) of the DFG.

REFERENCES

- Abia, C., Cunha, K., Cristallo, S., de Laverny, P., Domínguez, I., Recio-Blanco, A., Smith, V. V., & Straniero, O. 2011, *ApJ*, 737, L8
- Abia, C., Recio-Blanco, A., de Laverny, P., Cristallo, S., Domínguez, I., & Straniero, O. 2009, *ApJ*, 694, 971
- Abia, C., et al. 2010, *ApJ*, 715, L94
- Alves-Brito, A., Karakas, A. I., Yong, D., Meléndez, J., & Vásquez, S. 2011, *A&A*, 536, A40
- Alves-Brito, A., Yong, D., Meléndez, J., Vásquez, S., & Karakas, A. I. 2012, *A&A*, 540, A3
- Anders, E., & Grevesse, N. 1989, *Geochim. Cosmochim. Acta*, 53, 197
- Asplund, M., Nordlund, Å., Trampedach, R., & Stein, R. F. 1999, *A&A*, 346, L17
- Bell, R. A., Eriksson, K., Gustafsson, B., & Nordlund, A. 1976, *A&AS*, 23, 37
- Caffau, E., Ludwig, H.-G., Steffen, M., Freytag, B., & Bonifacio, P. 2011, *Sol. Phys.*, 268, 255
- Carney, B. W., Latham, D. W., Stefanik, R. P., Laird, J. B., & Morse, J. A. 2003, *AJ*, 125, 293
- Cayrel, R. 1988, in *IAU Symposium, Vol. 132, The Impact of Very High S/N Spectroscopy on Stellar Physics*, ed. G. Cayrel de Strobel & M. Spite, 345
- Collet, R., Asplund, M., & Trampedach, R. 2007, *A&A*, 469, 687
- Cunha, K., & Smith, V. V. 2005, *ApJ*, 626, 425
- Cunha, K., Smith, V. V., & Gibson, B. K. 2008, *ApJ*, 679, L17
- Cunha, K., Smith, V. V., Lambert, D. L., & Hinkle, K. H. 2003, *AJ*, 126, 1305

Dobrovolskas, V., Kucinskas, A., Ludwig, H. G., Caffau, E., Klevas, J., & Prakačavičius, D. 2010, in *Nuclei in the Cosmos*.

Forestini, M., Goriely, S., Jorissen, A., & Arnould, M. 1992, *A&A*, 261, 157

González Hernández, J. I., et al. 2008, *A&A*, 480, 233

Goorvitch, D. 1994, *ApJS*, 95, 535

Heger, A., Kolbe, E., Haxton, W. C., Langanke, K., Martínez-Pinedo, G., & Woosley, S. E. 2005, *Physics Letters B*, 606, 258

Hinkle, K., Wallace, L., & Livingston, W. 1995, *PASP*, 107, 1042

Ivanauskas, A., Kucinskas, A., Ludwig, H. G., & Caffau, E. 2010, in *Nuclei in the Cosmos*.

Jorissen, A., Smith, V. V., & Lambert, D. L. 1992, *A&A*, 261, 164

Kaeufel, H.-U., et al. 2004, in *Society of Photo-Optical Instrumentation Engineers (SPIE) Conference Series*, Vol. 5492, *Society of Photo-Optical Instrumentation Engineers (SPIE) Conference Series*, ed. A. F. M. Moorwood & M. Iye, 1218–1227

Kobayashi, C., Izutani, N., Karakas, A. I., Yoshida, T., Yong, D., & Umeda, H. 2011a, *ApJ*, 739, L57

Kobayashi, C., Karakas, A. I., & Umeda, H. 2011b, *MNRAS*, 414, 3231

Kurucz, R. 1994, *Solar abundance model atmospheres for 0,1,2,4,8 km/s*. Kurucz CD-ROM No. 19. Cambridge, Mass.: Smithsonian Astrophysical Observatory, 1994., 19

Lucatello, S., Masseron, T., Johnson, J. A., Pignatari, M., & Herwig, F. 2011, *ApJ*, 729, 40

Ludwig, H.-G., Caffau, E., Steffen, M., Freytag, B., Bonifacio, P., & Kučinskas, A. 2009, *Mem. Soc. Astron. Italiana*, 80, 711

Meynet, G., & Arnould, M. 2000, *A&A*, 355, 176

Nissen, P. E., & Schuster, W. J. 2010, *A&A*, 511, L10

—. 2011, *A&A*, 530, A15

Pandey, G. 2006, *ApJ*, 648, L143

Recio-Blanco, A., de Laverny, P., Worley, C., Santos, N. C., Melo, C., & Israelian, G. 2012, *A&A*, 538, A117

Renda, A., et al. 2004, *MNRAS*, 354, 575

Schuler, S. C., Cunha, K., Smith, V. V., Sivarani, T., Beers, T. C., & Lee, Y. S. 2007, *ApJ*, 667, L81

Shetrone, M. D. 1996, *AJ*, 112, 1517

Shetrone, M. D., Smith, G. H., Briley, M. M., Sandquist, E., & Kraft, R. P. 1999, *PASP*, 111, 1115

Smith, V. V., Cunha, K., Ivans, I. I., Lattanzio, J. C., Campbell, S., & Hinkle, K. H. 2005, *ApJ*, 633, 392

Snedden, C. 1973, *ApJ*, 184, 839

Uttenthaler, S., Aringer, B., Lebzelter, T., Käufel, H. U., Siebenmorgen, R., & Smette, A. 2008, *ApJ*, 682, 509

Werner, K., Rauch, T., & Kruk, J. W. 2005, *A&A*, 433, 641

Woosley, S. E., & Haxton, W. C. 1988, *Nature*, 334, 45

Woosley, S. E., & Weaver, T. A. 1995, *ApJS*, 101, 181

Yong, D., Meléndez, J., Cunha, K., Karakas, A. I., Norris, J. E., & Smith, V. V. 2008, *ApJ*, 689, 1020

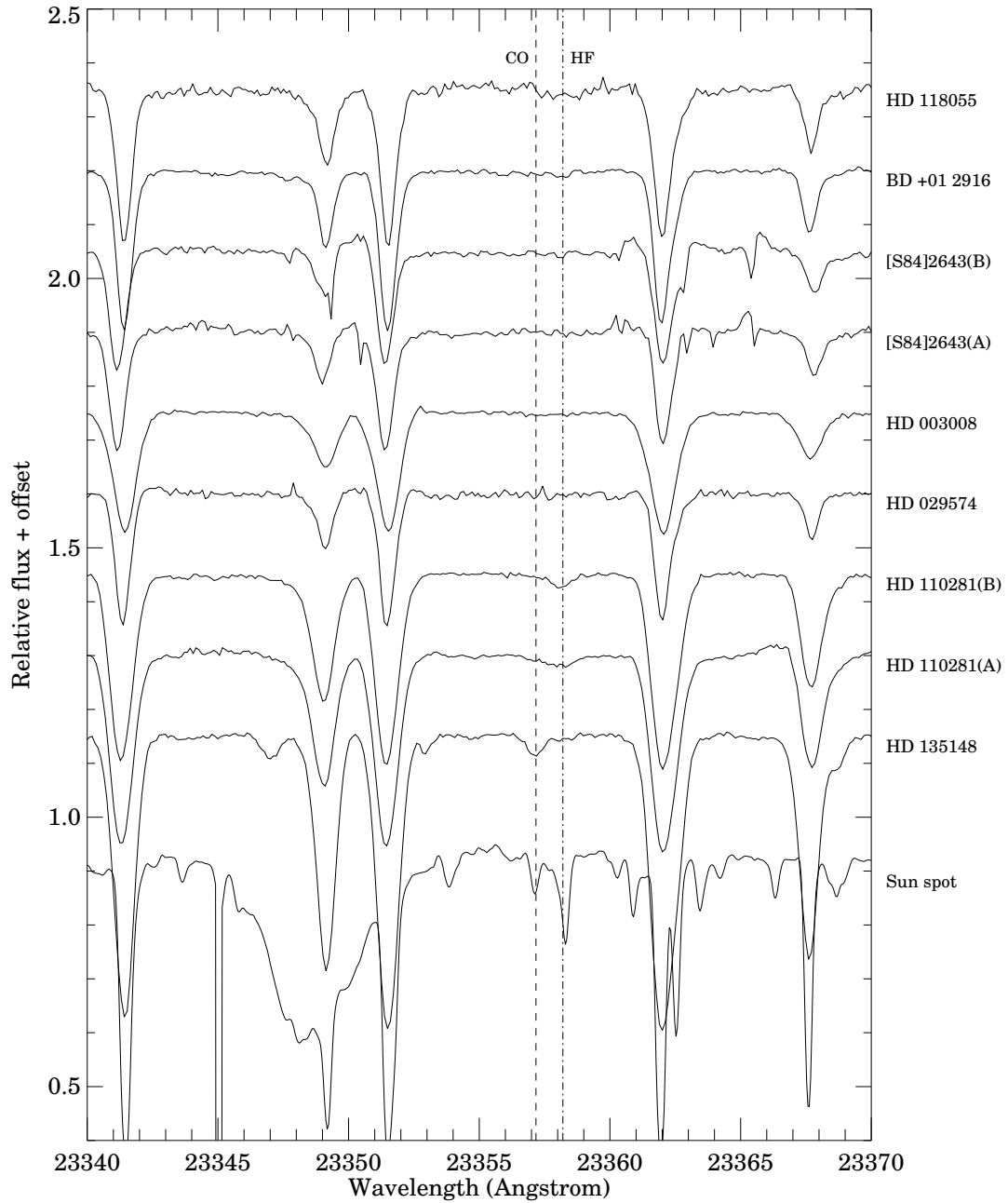


Fig. 1.— Overview of the HF-region spectra for all exposures of the programs stars. The position of the HF R9 line and the closely C¹⁷O are indicated by dash-dotted and dashed lines respectively. A *K*-band Sun spot spectrum in this area is also plotted for comparison.

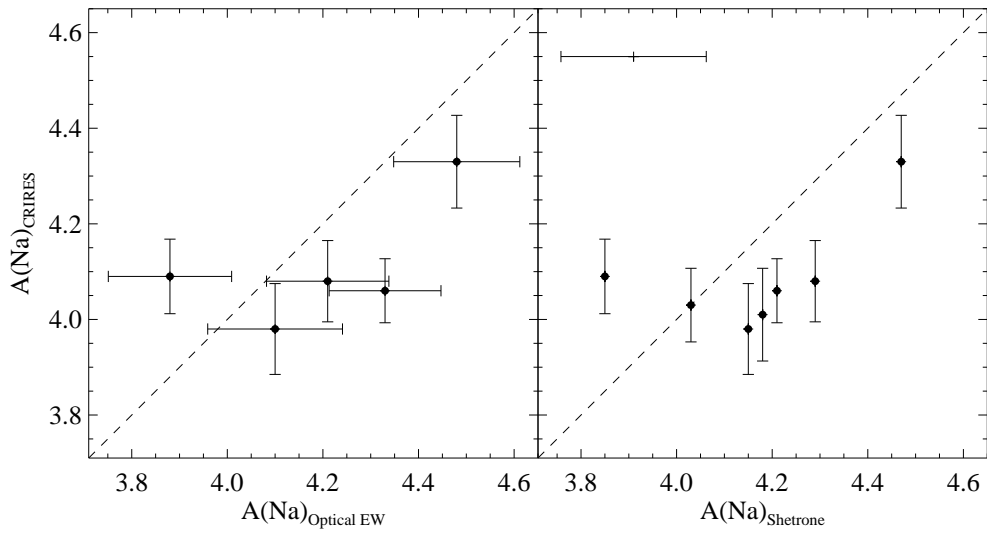


Fig. 2.— Na abundances derived from CRILES spectra are compared with those re-derived using Shetrone (1996)’s EWs measured from optical spectra (left), and the original results provided by Shetrone (1996) (right). Two objects with no EWs available from the literature are not included in the left plot.

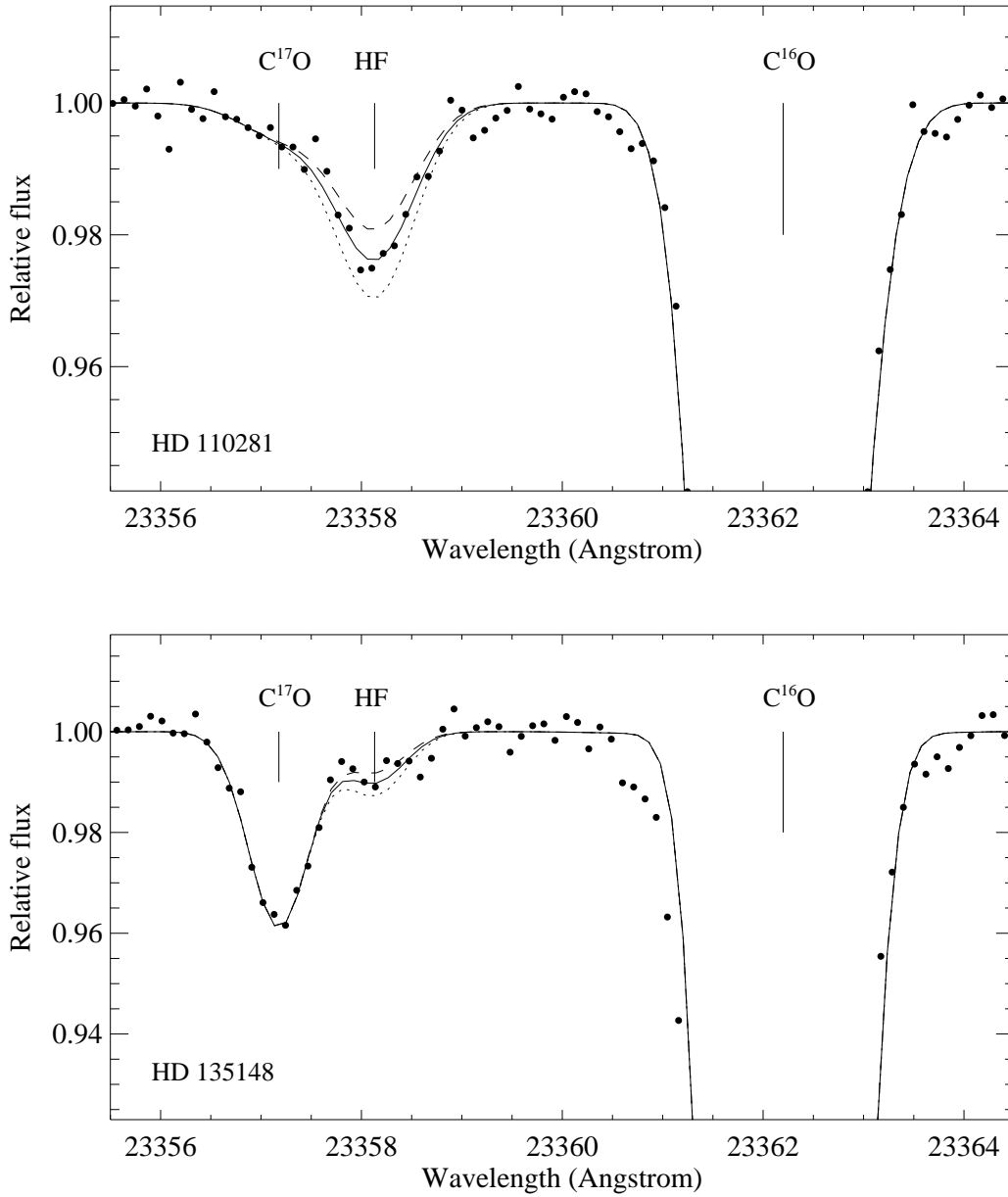


Fig. 3.— Sample spectra with spectral synthesis of HF line at 23358 Å of HD 110281 and HD 135148, the two program stars with clear HF detections. Black dots are observed data points. Solid lines refer to the synthetic spectra with the adopted $A(F)$, with dashed lines and dotted lines referring to synthetic spectra with $\Delta A(F) = \pm 0.1$ dex. Note that for the CH star HD 135148, the C¹⁷O line to the blue side of the HF line is clearly detected and also fitted.

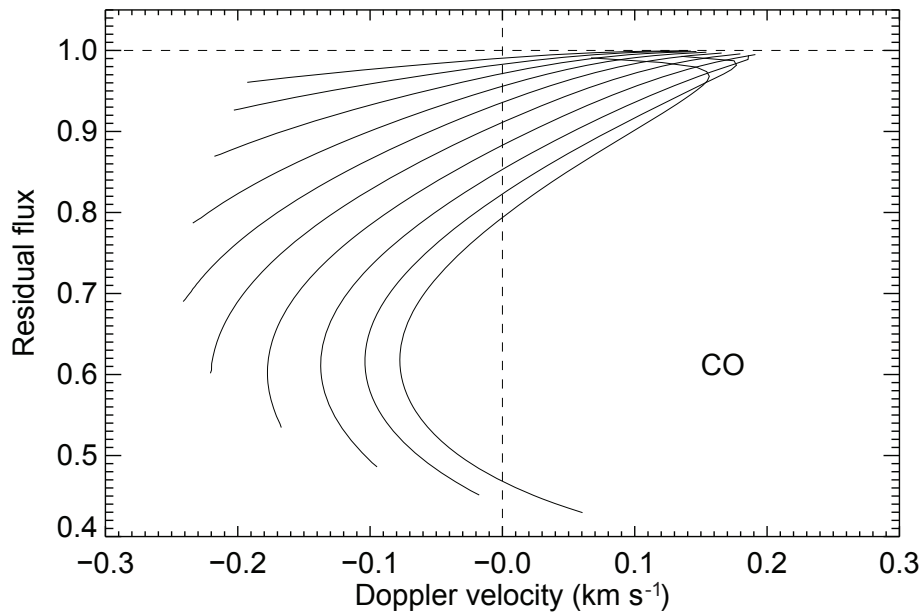


Fig. 4.— Line bisectors of typical CO lines (solid lines) of different strength in the HF region. The line synthesis was done at constant C/O ratio. Zero Doppler velocity corresponds to the laboratory wavelength.

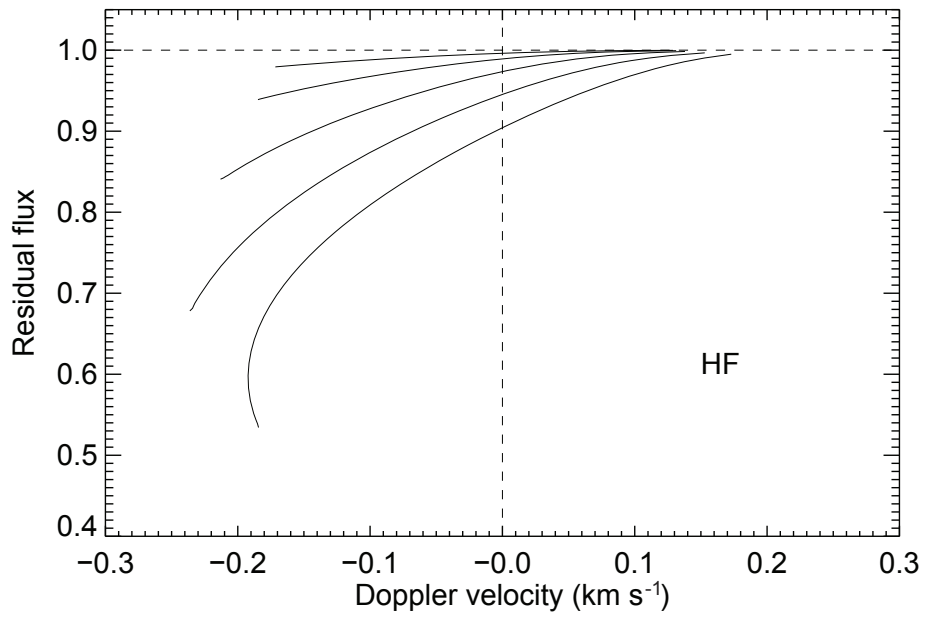


Fig. 5.— Line bisectors of the HF R9 line (solid lines) of different strength. Zero Doppler velocity corresponds to the laboratory wavelength

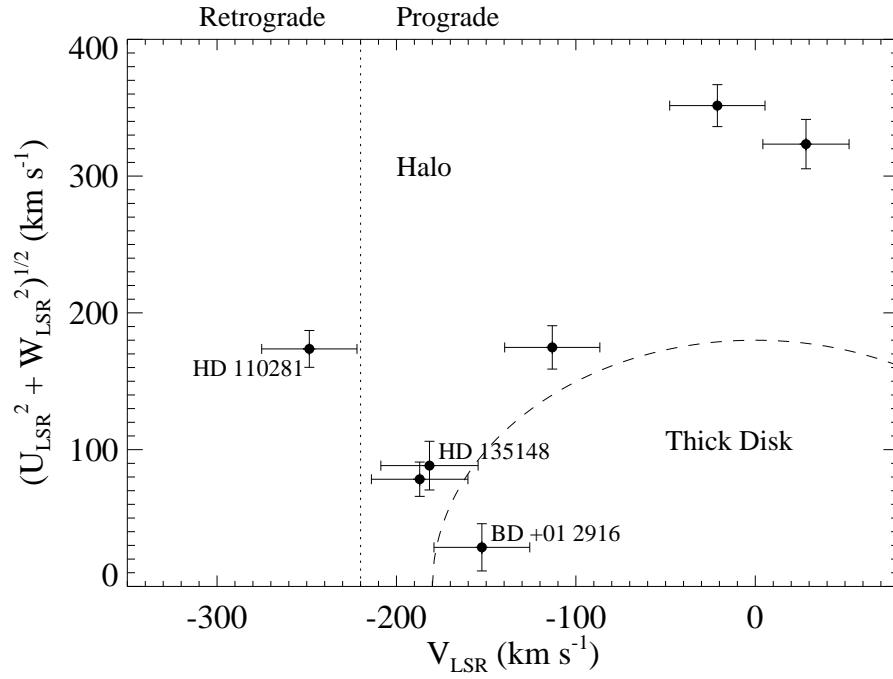


Fig. 6.— Toomre diagram of the program stars. The long-dashed line corresponds to $V_{\text{total}} = 180$ km s⁻¹. The short-dashed line indicates zero rotation in the Milky Way. Two objects with HF detections, HD 110281 (with retrograde rotation) and HD 135148 (the CH-star), and BD +01 2916 (identified as a thick disk star) are marked in the plot.

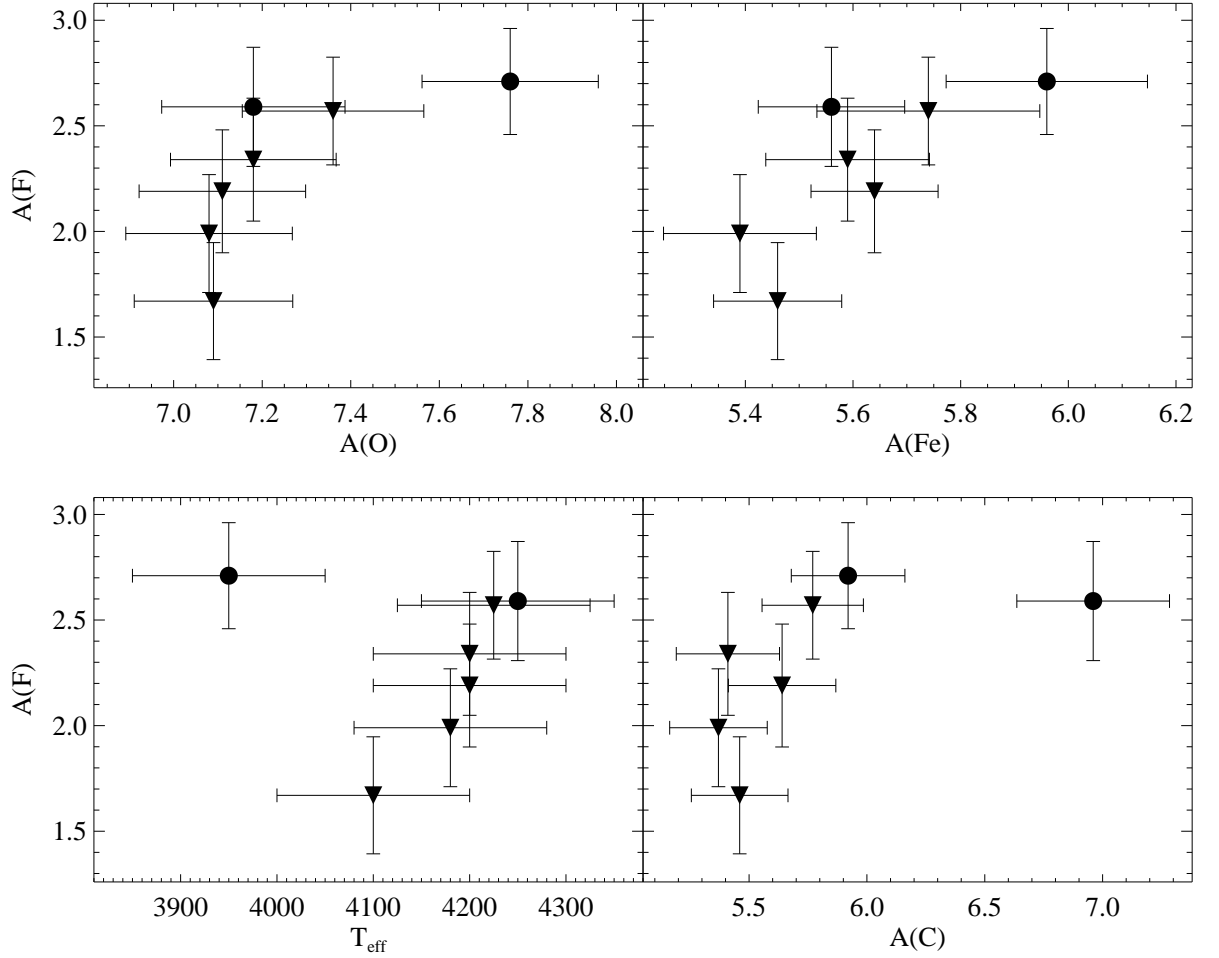


Fig. 7.— Variances of the F abundance along T_{eff} , abundances of C, O and Fe. The filled circles with error bars refer to HD 110281 and HD 135148, and all upside-down filled triangles correspond to the program stars with 2- σ upper limits of F for the cases in which the HF line is not detected. 1- σ errors are overplotted to the observed data.

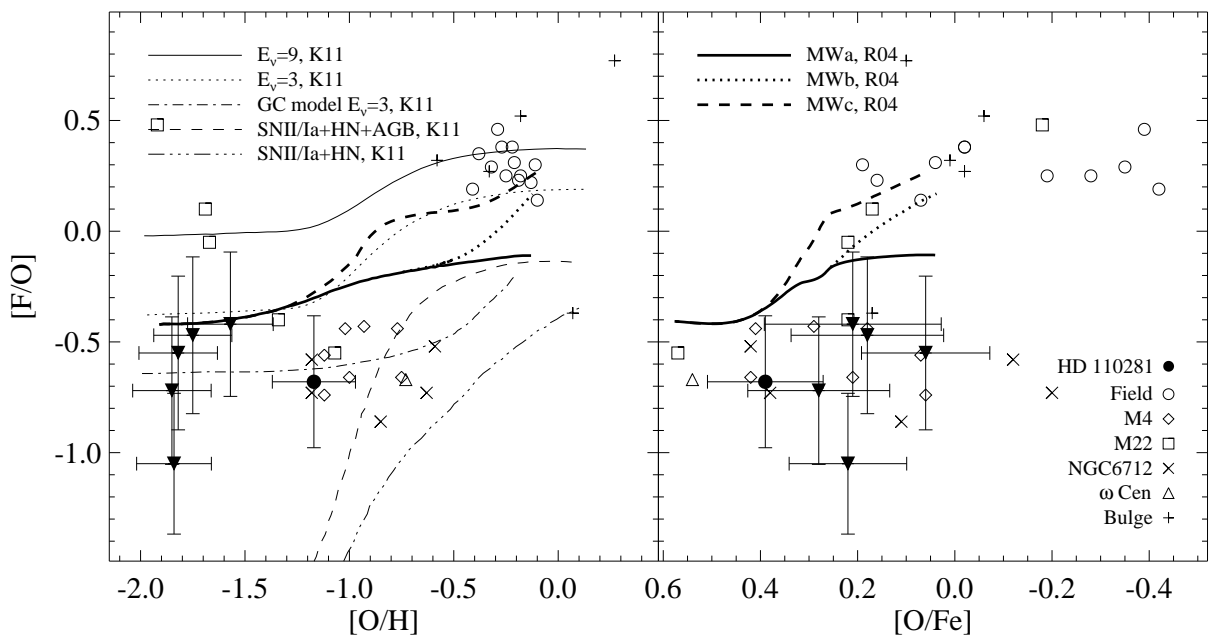


Fig. 8.— The F yields in the form of $[F/O]$ as a function of $[O/H]$ and $[O/Fe]$. Models of Renda et al. (2004; thick lines) and Kobayashi et al. (2011a; thin lines) are shown, with line identifications described in the plot and text. Observations of various giants are also included: open circles for field K and M giants from Cunha et al. (2003), and Cunha & Smith (2005); diamonds, squares, crosses, and triangles for globular cluster giants from M4 (Smith et al. 2005), M22 (Alves-Brito et al. 2012), NGC6712 (Yong et al. 2008), and ω Cen (Cunha et al. 2003), respectively; pluses for bulge giants from Cunha et al. (2008). Filled symbols are the same as in Figure 7, except that the CH-star HD 135148 is not included in the plot due to its peculiarly enhanced F abundances as explained in the context. All abundances of models and observations are calibrated to the same set of solar abundances from Anders & Grevesse (1989).

Table 1: Stellar Parameters and Abundances of the Sample.

Star	T_{eff}	$\log g$	[Fe/H]	$\xi \text{ km s}^{-1}$	FWHM ^a	S/N	A(C)	A(O)	A(F)	A(Na)	A(Mg)	A(Al)	A(Eu)
BD +01 2916	4200	0.10	-1.88	2.10	0.709	357.3	5.64	7.11	<2.19	4.08	6.21	4.46	-1.13
HD 003008	4100	0.10	-2.06	1.90	1.030	591.8	5.46	7.09	<1.67	3.98	6.33	4.21	-1.21
HD 029574	4200	0.10	-1.93	1.75	0.658	226.8	5.41	7.18	<2.34	4.01	6.30	4.40	-0.95
HD 110281	3950	0.20	-1.56	2.43	0.996	462.5	5.92	7.76	2.71	4.33	6.42	4.70	-0.46
HD 118055	4225	0.70	-1.78	1.63	0.687	163.6	5.77	7.36	<2.57	4.03	6.20	4.58	-0.86
HD 135148	4250	0.70	-1.96	2.40	0.899	360.2	6.96	7.18	2.59	4.06	6.02	4.59	— ^b
[S84] 2643	4180	0.40	-2.13	1.65	0.735	316.3	5.37	7.08	<1.99	4.09	6.07	4.50	— ^b

- 31 -

^aFWHM of the spectral lines of the sample stars (in mÅ), based on CO line measurements.

^bNo Eu line or EW measurement is available for this object from Shetrone (1996).

Table 2: 3D Abundance Corrections^a on the HF R9 and Forbidden Oxygen Lines.

T_{eff}	$\log g$	HF R9		[O I] 6300Å		[O I] 6363Å		3D model ^b
3886	1.0	-0.02	-0.03	0.00	0.01	0.00	0.01	d3t36g10mm20n02
4001	1.5	-0.03	-0.03	0.00	0.01	0.00	0.01	d3t40g15mm20n01
4478	2.5	-0.16	-0.12	-0.01	-0.01	-0.01	-0.01	d3t45g25mm20n02
5024	2.5	-0.42	-0.52	0.00	-0.02	0.00	-0.02	d3t50g25mm20n01

^aLeft columns give 3D – 1D, right columns 3D – ⟨3D⟩, in dex.

^bAll models assume $[M/H] = -2.0$, and $[\alpha/Fe] = +0.4$.